Basal-plane slip systems and polymorphic phase transformation in Ti_2AlC and Ti_2AlN: a first-principles study

2006 J. Phys.: Condens. Matter 18 6183

(http://iopscience.iop.org/0953-8984/18/27/002)

INSTITUTE OF PHYSICS PUBLISHING JOURNAL OF PHYSICS: CONDENSED MATTER

J. Phys.: Condens. Matter **18** (2006) 6183–6192 doi:10.1088/0953-8984/18/27/002

Basal-plane slip systems and polymorphic phase transformation in Ti_2AlC and Ti_2AlN: a first-principles study

Ting Liao[1,2], **Jingyang Wang**[1,3] **and Yanchun Zhou**[1]

[1] High-performance Ceramic Division, Shenyang National Laboratory for Materials Science, Institute of Metal Research, Chinese Academy of Sciences, Shenyang 110016, People's Republic of China
[2] Graduate School of Chinese Academy of Sciences, Beijing 100039, People's Republic of China
[3] International Centre for Materials Physics, Institute of Metal Research, Chinese Academy of Sciences, Shenyang 110016, People's Republic of China

Received 10 November 2005
Published 23 June 2006
Online at stacks.iop.org/JPhysCM/18/6183

Abstract

Deformation modes are studied for two basal-plane slip systems, $[1\bar{2}10](0001)$ and $[\bar{1}010](0001)$, in ternary-layered Ti_2AlC and Ti_2AlN ceramics using the first-principles plane-wave pseudopotential total energy method. Based on the theoretical stress–strain curves, the $[\bar{1}010](0001)$ slip system leads to smaller ideal shear strength compared to the $[1\bar{2}10](0001)$ mode, implying that the $[\bar{1}010](0001)$ slip system is predominant to the mechanical properties of these ternary-layered compounds. Bond-length relaxations are examined for materials strained from elasticity to structural instability. Interatomic bonds are demonstrated to respond to shear strain inhomogeneously because of different bonding strengths. The slips of atomic planes are determined by the failure of weak Ti–Al bonds. In addition, we predict a polymorphic phase transformation along the $[1\bar{2}10](0001)$ shear deformation path. For the $[\bar{1}010](0001)$ slip system, in contrast, no polymorphic phase transformation is observed because TiC slabs do not hold the original NaCl-type structure and, in addition, Al layers change from a hexagonal to a cubic stacking in the shear deformed lattice. In other words, the structural units undergo different atomic configurations from those in the two polymorphs under applied shear strain.

(Some figures in this article are in colour only in the electronic version)

1. Introduction

Ternary-layered carbides or nitrides with the general formula $T_{n+1}AX_n$ (where $n = 1$–3, T is an early transition metal, A is an A-group element, mostly from groups IIIA and IVA, and X is either C and/or N) are best described as thermodynamically stable polycrystalline

ceramics. These compounds are found to exhibit many of the best attributes of both metals and high-performance ceramics, such as low density, high thermal and electrical conductivities, good thermal shock resistance and damage tolerance, excellent oxidation resistance, high elastic stiffness, and easy machinability at room temperature [1]. The unusual combination of properties makes these ternary ceramics promising candidates for high-temperature structural applications. Ti_2AlC is of particular interest in this family. As the most stable phase in the Ti–Al–C system, Ti_2AlC has a comparatively low density (4.11 g cm^{-3}) compared to other layered ternary members [2]. The ability to form a protective Al_2O_3 scale at elevated temperatures provides Ti_2AlC with excellent high-temperature oxidation resistance [3]. With one more valence electron in the formula, Ti_2AlN is elastically stiffer than Ti_2AlC without abating other magnificent attributes [4][4].

As expected from the layered crystal structure with space group $P6_3/mmc$, deformations in Ti_2AlC and Ti_2AlN are limited by a lack of sufficient easy slip systems (rather than the five independent slip systems needed for arbitrary deformation) and are quite anisotropic [5]. Transmission electron microscope observations have been performed to study the room-temperature deformation of macro-grained Ti_3SiC_2 ceramic [6, 7]. The results showed that deformation of individual grains included the generation and conservative motions of basal-plane dislocations with a Burgers vector of $1/3[11\bar{2}0]$. Therefore, only the basal-plane slip was favoured in these ternary-layered compounds.

On the (0001) basal plane, slips may be activated in either the $[1\bar{2}10](0001)$ or the $[\bar{1}010](0001)$ direction under different loading conditions. It is still not clear which slip system is more operative and essential to the mobility of basal-plane dislocations. For the $T_{n+1}AX_n$ ceramics, an understanding of the basal-plane sliding modes is the key to explaining micro-scale ductility and plasticity at room temperature. Generally speaking, the very low mobility of dislocation kinks in covalently bonded materials is determined by the very high bond-breaking energy under a large shear strain. Furthermore, the bond-breaking energy involved in plastic deformation and the bond-restoring energy under elastic shear strain essentially go together in these materials. This reason indicates that the response of well-localized covalent bonds to shear strain is the crucial factor in determining plasticity. Recent advances in both computational and methodological capabilities have made it possible to perform an *ab initio* calculation on the shear deformation from elasticity to structural instability with reasonable accuracy; examples include [8–11].

Like the elastic constants, ideal strength is material-specific and can be determined accurately by first-principles calculations. It defines the upper bound strength that a particular material can possibly have, and is decided by the limit of structural stability. Nanoindentation experiments suggested that stress could approach the ideal shear strength in a small volume under the nanoindenter [12]. The aim of the present work is to investigate the deformation mechanisms for materials strained from elasticity to structural instability along the two selected basal-plane slip directions. It is our ambition to reveal the origin of ductility and machinability of ternary-layered carbides and nitrides.

2. Computational details

Density functional calculations were performed based on the CASTEP [13] code, in which the plane-wave pseudopotential total energy method was adopted. The interactions between the core region and valence electrons of the atoms were described by the Vanderbilt-type ultrasoft pseudopotential [14]. In addition, the electronic exchange–correlation energy was treated using

[4] For Ti_2AlN, the elastic moduli are calculated in accordance with the same computational method of [4].

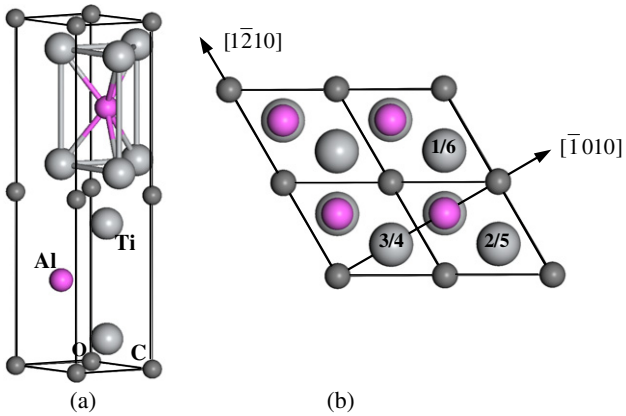

Figure 1. Crystal structure of Ti_2AlC, in which the Ti_6Al prism is highlighted and connected by bold bonds. A $2 \times 2 \times 1$ supercell projected onto the (0001) plane is also displayed, with the two slip directions indicated.

the generalized gradient approximation (GGA-PW91) [15]. The plane-wave basis set cutoff was chosen as 450 eV for all cases. The numerical integration of the Brillouin zone was performed using a discrete $10 \times 10 \times 2$ Monkhorst–Pack k-point sampling for equilibrium structures [16]. A larger number of k-points ($12 \times 12 \times 4$) was chosen to sample the Brillouin zone for those strained unit cells. This choice arose from two reasons: one was the reduced symmetry of the sheared unit cell, and the other was due to the change of the Brillouin zone shape. These parameters ensured good convergences of both total energy and geometrical configurations. The convergence tolerances for the geometry optimization of an unstrained unit cell were selected with a difference in total energy within 5×10^{-6} eV/atom, a maximum ionic Hellmann–Feynman force within 0.01 eV $Å^{-1}$, a maximum ionic displacement within 5×10^{-4} Å, and a maximum stress within 0.1 GPa.

In the present study, the ideal stress–strain relationship was obtained by deforming the crystals from elasticity to structural instability. A series of incremental shear strains in the [1$\bar{2}$10] or the [$\bar{1}$010] direction on the (0001) plane were applied to the unit cell under constant-strain-constraint conditions. To ensure that the unit cell was in a uniaxial stress state, we relaxed all cell constants and internal degrees of freedom, i.e. internal atomic coordinates, until the calculated Hellmann–Feynman stresses are less than 0.2 GPa, while constraining the applied shear strain. The ideal shear strength was defined as the first maximum shear stress achieved with applied shear strain.

It is necessary to inspect whether a single unit cell is good enough for the convergence of stress, especially for ideal strength, with respect to the cell dimension. We doubled the cell size along the c axis and calculated the ideal strengths for a strained $1 \times 1 \times 2$ Ti_2AlC supercell along the [1$\bar{2}$10](0001) and [$\bar{1}$010](0001) directions. The stress differences between the single unit cell and the $1 \times 1 \times 2$ supercell are 0.11 and 0.09 GPa for [1$\bar{2}$10](0001) and [$\bar{1}$010](0001) shear modes, respectively. Therefore, good stress convergence was achieved using a single unit cell.

3. Results and discussions

3.1. Basal-plane slip systems

Figures 1(a) and (b) show the Ti_2AlC unit cell and a $2 \times 2 \times 1$ supercell projected along the [0001] direction, respectively. The two slip directions that were studied are indicated

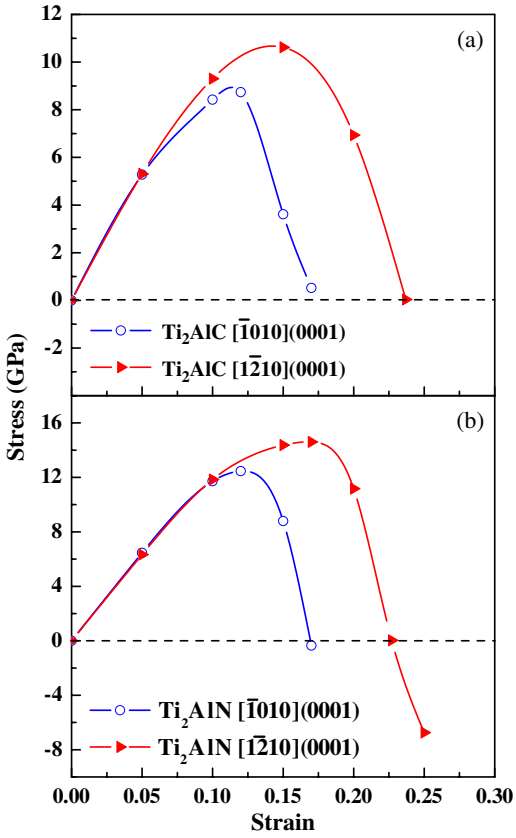

Figure 2. Calculated shear stresses versus strain along the $[1\bar{2}10](0001)$ and $[\bar{1}010](0001)$ slip systems for (a) Ti_2AlC and (b) Ti_2AlN. Solid triangles represent data for the $[1\bar{2}10](0001)$ slip system, and empty circles are for $[\bar{1}010](0001)$.

in figure 1(b). The crystal structure of ternary Ti_2AlC can be described as NaCl-type Ti_2C slabs being interleaved by close-packed Al atomic planes. Electronic structure investigations have shown that the coupling between the Ti_2C slabs and the Al atomic planes were relative weak [4, 18–20]. The Ti_6Al triangular prism is highlighted by bold bonds in figure 1(a) in order to analyse the response of Ti–Al bonds to shear deformation conveniently.

Calculated shear stresses at various strains are displayed in figures 2(a) and (b) for Ti_2AlC and Ti_2AlN, respectively. Maximum stress is achieved at a strain of around 0.15 for the $[1\bar{2}10](0001)$ shear path and 0.12 for the $[\bar{1}010](0001)$ shear path for Ti_2AlC. Material under the latter shear deformation path undergoes stress relaxation earlier. Furthermore, the ideal shear strength differs by 3 GPa for the two shear modes studied. The values are 12 and 9 GPa for the $[1\bar{2}10](0001)$ and $[\bar{1}010](0001)$ directions, respectively. Ti_2AlN shows similar ideal stress–strain relationships to Ti_2AlC, except for the higher shear strengths. The ideal shear strengths are 14 and 11 GPa along the $[1\bar{2}10](0001)$ and $[\bar{1}010](0001)$ directions, respectively, as shown in figure 2(b). Comparing the ideal stress–strain relationships of the two competing strain paths, i.e. along the $[1\bar{2}10](0001)$ and $[\bar{1}010](0001)$ directions, the latter strain path leads more easily to structural instability. Therefore, the ultimate strengths of Ti_2AlC and Ti_2AlN should be determined by the lattice stability under the $[\bar{1}010](0001)$ shear deformation.

Table 1. The internal strain parameter are compared between the $[1\bar{2}10](0001)$ and $[\bar{1}010](0001)$ deformation modes for Ti_2AlC under various shear amplitudes. Both Ti–Al and Ti–C bonds are taken into account.

		ζ_{AB} at various shear strains			
Bonds	Slip systems	0.05	0.10	0.12	0.15
Ti–Al	$[1\bar{2}10](0001)$	−0.317	−0.330	−0.334	−0.352
	$[\bar{1}010](0001)$	−0.336	−0.466	−0.555	−0.755
Ti–C	$[1\bar{2}10](0001)$	0.627	0.687	0.704	0.759
	$[\bar{1}010](0001)$	0.665	0.734	0.800	0.974

Previous investigations revealed that the mechanical properties of $T_{n+1}AX_n$ phases were determined by the weak T–A bonds. To understand the differences in ideal strengths between Ti_2AlC and Ti_2AlN, we studied the changes in Ti–Al bonding strength in these compounds. A nitrogen atom provides one more valence electron to the Ti_6N octahedron in Ti_2AlN compared to the carbon atom in Ti_2AlC. If the enhancement of the valence electron density could strengthen the Ti–Al bonding, the strength of the material can be effectively increased. Electronic structure analysis showed that the Ti–Al bonding states shift from −2.41 to −0.04 eV below the Fermi level (E_F) in Ti_2AlC to lower energy levels, ranging from −3.01 to −0.55 eV below the E_F in Ti_2AlN. This indicates a strengthening of the Ti–Al bonds, and thereafter enhances the ideal strengths of Ti_2AlN.

In order to better understand the deformation mechanism, we studied the bond-length relaxations in the shear-deformed lattice. Due to different bonding strengths, inhomogeneous relaxations of interatomic bonds are investigated quantitatively by the internal displacement parameter ζ [21], defined by:

$$\zeta_{AB} = \frac{1}{n_{AB}} \sum_{i=1}^{n_{AB}} (d_{AB,i} - d^*_{AB,i})/(d^\circ_{AB,i} - d^*_{AB,i}) \tag{1}$$

where $d^\circ_{AB,i}$, $d_{AB,i}$ and $d^*_{AB,i}$ correspond to the bond lengths in the unstrained unit cell and shear strained unit cells with and without bond-length relaxations, respectively, and n_{AB} is the number of each type of bond. According to the definition, $\zeta_{AB} = 0$ corresponds to the case of homogeneous deformation; $\zeta_{AB} = 1$ implies an ideal rigid bond upon deformation; $\zeta_{AB} > 0$ suggests a recovery trend from the applied homogeneous deformation, while $\zeta_{AB} < 0$ means an inhomogeneous relaxation to accommodate deformation.

Table 1 summarizes the calculated ζ_{AB} at different shear strains for Ti_2AlC. The ζ_{Ti-Al} yields a negative value and deviates from zero further under increased shear strain. This indicates that the Ti–Al bond accommodates the applied shear deformation effectively. Furthermore, the Ti–Al bond experiences larger relaxation in the $[\bar{1}010](0001)$ shear path compared to along the other shear direction, as indicated by the larger absolute values of ζ_{Ti-Al}. This suggests that the Ti–Al bond sustains larger strain and reaches its limit of structural stability earlier for strain along the $[\bar{1}010]$ direction. The ζ_{Ti-C}, on the other hand, has a positive value, which means a more rigid character of the Ti–C bond. Along the $[\bar{1}010](0001)$ shear path, the Ti–C bond has larger ζ_{Ti-C} than that along the $[1\bar{2}10](0001)$ shear path. Beyond the strain yielding maximum stress, i.e. a strain of 0.15, the computed ζ_{Ti-C} is 0.974 for the $[\bar{1}010](0001)$ shear mode, which is a value very close to that of an ideal rigid bond. Therefore, the Ti–C bond recovers rigidly, in contrast to the Ti–Al bond conducting significant relaxation.

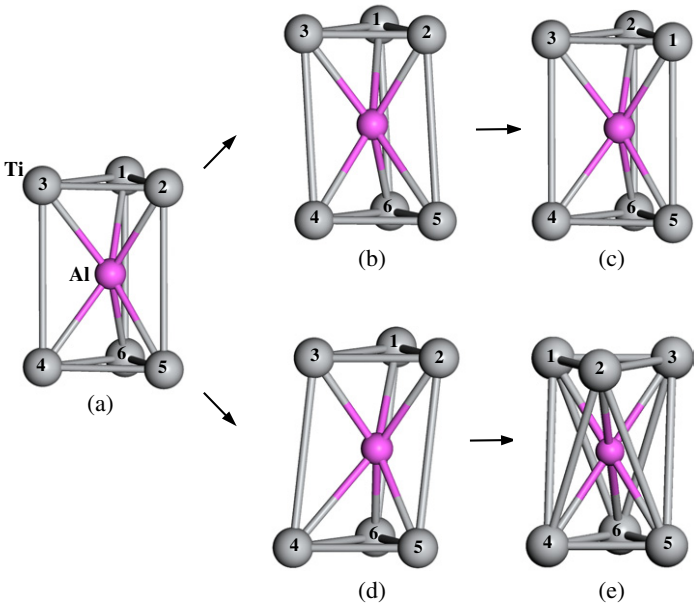

Figure 3. Configuration changes of a Ti_6Al prism. The unstrained substructure is shown in (a), whereas (b) corresponds to the structure under an applied shear strain of 0.1 for the $[1\bar{2}10](0001)$ shear mode, while (c) is the final relaxed configurations of Ti_6Al after removing the constant-shear-strain constraint. (d) and (e) figures are similar to (b) and (c), except for the $[\bar{1}010](0001)$ shear modes. The bond lengths in configurations (b) and (d) are listed in table 2.

Table 2. Bond lengths in relaxed Ti_6Al prisms under applied 0.1 shear strain for $[1\bar{2}10](0001)$ and $[\bar{1}010](0001)$ shear modes.

Slip systems	Bond lengths of Ti–Al (Å)		
$[1\bar{2}10](0001)$	3.088 (Ti^1–Al)	2.767 (Ti^2–Al)	2.816 (Ti^3–Al)
	2.767 (Ti^6–Al)	3.088 (Ti^5–Al)	2.816 (Ti^4–Al)
$[\bar{1}010](0001)$	2.944 (Ti^1–Al)	2.944 (Ti^2–Al)	2.761 (Ti^3–Al)
	2.796 (Ti^6–Al)	2.796 (Ti^5–Al)	3.169 (Ti^4–Al)

Figure 3 presents the evolution of a Ti_6Al trigonal prism under a shear strain of 0.1, and the corresponding bond lengths are listed in table 2. For an applied homogeneous shear strain, the Ti_6Al prism is distorted by breaking its trigonal symmetry. With respect to energy minimization, Ti–Al bonds undergo different bond-length relaxations. For the $[1\bar{2}10](0001)$ shear mode, the bond-length relaxations centre on the Ti^1–Al and Ti^5–Al bonds, as shown in figure 3(b). In contrast, other Ti–Al bonds change negligibly. Figure 3(d) displays the optimized structure of the Ti_6Al configuration along the $[\bar{1}010](0001)$ shear path. Only the Ti^4–Al bond changes significantly. In figures 3(c) and (e), different coordination for the Al adjacent to Ti atoms is of the most interest. The Al atom retains its original trigonal prismatic coordination to Ti in figure 3(c), while it undergoes an octahedral coordination to Ti in figure 3(e). In the following section we will discuss that only the trigonal prismatic coordination corresponds to a polymorphic phase transformation along the $[1\bar{2}10](0001)$ shear path. Although the Ti–Al bonds are deformed differently along the two shear paths, a common

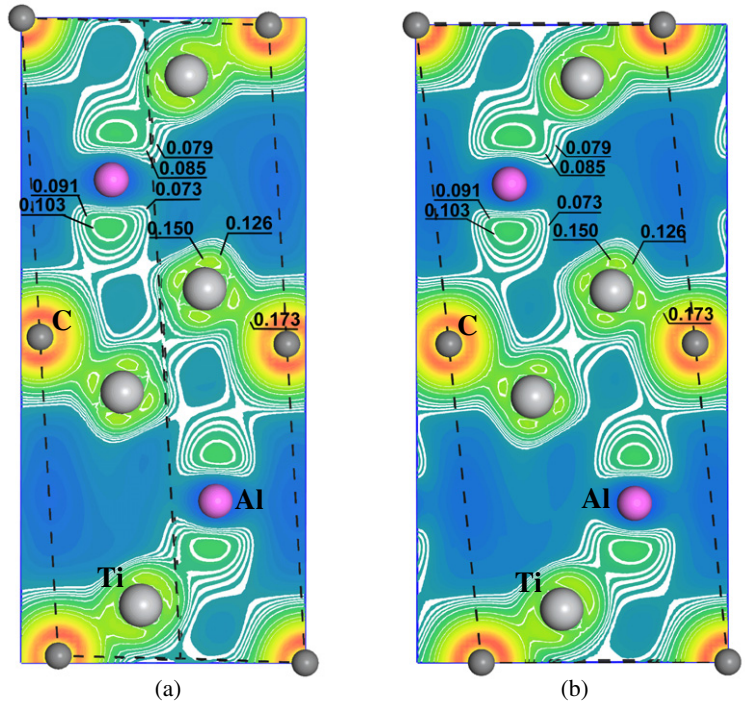

Figure 4. Valence electron density for Ti_2AlC at 0.1 shear strain for (a) the $(11\bar{2}0)$ planes for $[1\bar{2}10](0001)$ shear mode, and (b) the $(1\bar{2}10)$ planes for $[\bar{1}010](0001)$ shear mode. The contour lines range from 0.073 to 0.173 electrons $Å^{-3}$.

characteristic is addressed as follows: structural instability is determined only by failure of the Ti–Al bond. Moreover, under the same shear strain of 0.1, the Ti–Al bond stretches to a larger length, i.e. 3.169 Å, along the $[\bar{1}010](0001)$ strain path than that along the $[1\bar{2}10](0001)$ direction characterized by a value of 3.088 Å. The difference in bond length indicates an easier bond-breaking event in the $[\bar{1}010](0001)$ strain mode.

Electronic origins of bond relaxation and bond breaking are displayed by the valence charge densities on the $(1\bar{2}10)$ and $(11\bar{2}0)$ atomic planes for Ti_2AlC under $[\bar{1}010](0001)$ and $[1\bar{2}10](0001)$ deformations, respectively, as shown in figure 4. The valence electron concentration along the Ti–C bond shows a minor difference for material under the two strains, indicating that the Ti–C bonding is insensitive to shear deformation. Compared to the stable Ti–C bond, a weak Ti–Al bond responds more readily to shear strain. As shown in figures 3(b) and (d), only the significantly stretched Ti–Al bond, instead of all Ti–Al bonds, breaks under large shear strain. The gradually occurring bond breaking interprets the small critical slip resistance well in both slip modes. Besides, it can also be concluded that the Ti–Al bond sustains better stability along the $[1\bar{2}10](0001)$ shear path. This is the mechanism of higher ideal shear strength, as well as the larger critical strain leading to structural instability for the $[1\bar{2}10](0001)$ strain path.

3.2. Polymorphic phase transformation

Using first-principles calculation, Wang *et al* [17] reported that a polymorphic phase transformation occurred in Ti_3SiC_2 under large shear strain. Later, the shear-induced phase

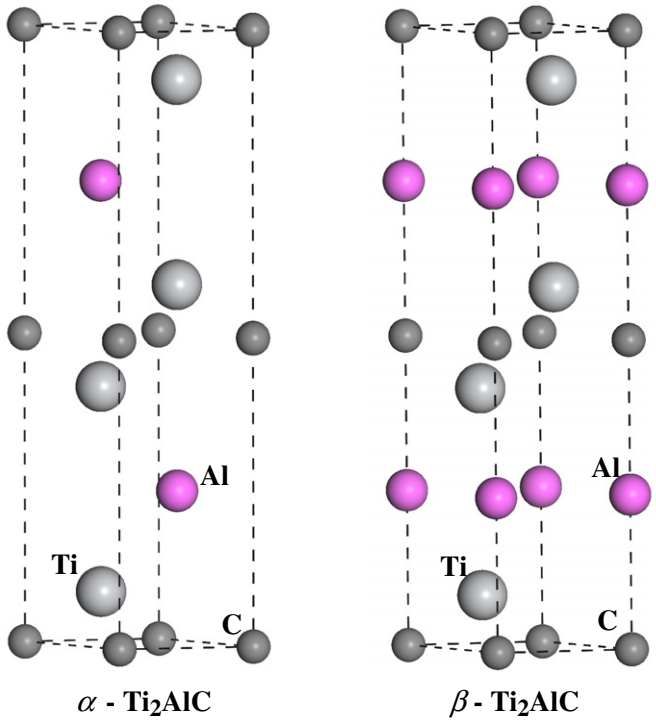

Figure 5. Crystal structures of the α- and β-Ti_2AlC polymorphs.

transformation of Ti_3GeC_2 was explored in light of theoretical predictions [22]. The crystal structures of Ti_2AlC/Ti_2AlN and Ti_3SiC_2/Ti_3GeC_2 are rather similar. Ti_3SiC_2/Ti_3GeC_2 consists of double layers of distorted edge sharing Ti_6C octahedra that are separated by close-packed Si/Ge atomic planes, and Ti_2AlC/Ti_2AlN consists of one Ti_6C/Ti_6N octahedra layer between two Al atomic planes. It is expected that Ti_2AlC/Ti_2AlN undergoes the same polymorphic phase transformation.

In order to study the possible phase transformation, the crystal structure was studied by a full optimization of the shear-strained unit cell by removing the constant-applied-shear-strain constraint. It is found that the strained Ti_2AlC lattice relaxes back to its equilibrium structure for a $[1\bar{2}10](0001)$ shear strain less than 0.24. In contrast, a new structure with space group $P6_3/mmc$ was reached for shear strain larger than 0.24. For comparison, the equilibrium structure is denoted as α-Ti_2AlC and the newly obtained structure is denoted as β-Ti_2AlC. Since the β modification is stable under strain perturbations, its crystal structure corresponds to a configuration with local minimum energy.

To distinguish the different structural configurations, the h–c notation was used. One can specify each layer in terms of the orientation of layers above and below it. A layer is said to be in hexagonal configuration and is denoted as 'h' if it is surrounded on either side by layers in a similar orientation. A layer is said to be in a cubic configuration and is denoted as 'c' if it is surrounded on either side by layers in different orientations. In the case of α-Ti_2AlC, its stacking sequence can be described as ABCAB in terms of the typical ABC notation. When described in the h–c notation, the stacking sequence can be written as hccch. The crystal structures of Ti_2AlC polymorphs are displayed in figure 5, and the relevant structural parameters are summarized in table 3. As can be seen from the crystal

Table 3. Calculated lattice parameters (in Å), total energy difference $\Delta E = E^{\alpha}_{\text{total}} - E^{\beta}_{\text{total}}$ (in eV/cell), volume (in $Å^3$/cell) and internal coordinates of Al atom for Ti_2AlC and Ti_2AlN polymorphs.

	Lattice parameters					
Compounds	a	c	c/a	ΔE_{total}	V	Wyckoff position of Al
α-Ti_2AlC	3.053	13.638	4.467	—	110.072	(2/3, 1/3, 1/4)
β-Ti_2AlC	3.037	13.797	4.543	−0.408	110.236	(0, 0, 1/4)
α-Ti_2AlN	2.984	13.503	4.525	—	104.155	(2/3, 1/3, 1/4)
β-Ti_2AlN	2.963	13.714	4.628	−0.407	104.244	(0, 0, 1/4)

structure, the polymorphic modification can be addressed by different stacking sequences of atomic planes along the c axis. In α-Ti_2AlC, both Ti and Al atoms are hexagonally stacked. While in β-Ti_2AlC, the Ti atom undergoes a cubic stacking, and Al layers remain the original hexagonal stacking sequence. The present β modification was isopointal with $FeWN_2$ [23] and $KNbS_2$ [24]. We are also concerned with the relative structural stability of the two phases. With respect to its lower total energy, α-Ti_2AlC is more stable than the β phase. The energy difference, i.e. 0.4 eV/unit cell, is rather small between the two polymorphs, and we expect the predicted β-phase to be identified in a sample synthesized under nonequilibrium conditions.

When a full optimization was performed on the shear-strained lattice of Ti_2AlC along the $[\bar{1}010](0001)$ path, the coordination environments of Ti, Al and C atoms changed greatly under the applied shear deformation. The Ti_2C slabs do not yield the NaCl-type structure anymore, and in addition Al layers undergo a transition from a hexagonal to a cubic stacking in terms of the h–c notation. The structural units show different atomic configurations from those in the polymorphs. For briefness, only the stacking environment of Al atoms is described in figure 3. It is believed that a c-stacking does not occur in any of these layered ternary carbides/nitrides. Once the applied strain takes place along the $[\bar{1}010](0001)$ direction, the hexagonal stacking configuration changes to a cubic stacking configuration for Al layers, leading to an octahedral coordination instead of trigonal prismatic coordination, for Al adjacent to Ti atoms, as illustrated in figure 3(e). As discussed before, the β modification requires hexagonal stacking for Al layers. Thereafter, the β-phase was not achieved along the $[\bar{1}010]$ direction.

4. Conclusion

We studied the deformation modes of two possible slip systems, $[1\bar{2}10](0001)$ and $[\bar{1}010](0001)$, for Ti_2AlC and Ti_2AlN, using the first-principles plane-wave pseudopotential total energy method. Deformation modes near the limit of structural stability were especially of concern and were compared for the two slip systems. The ultimate ideal shear strengths are about 25% and 21% smaller for $[\bar{1}010](0001)$ than those for $[1\bar{2}10](0001)$, respectively. The results suggest that the $[\bar{1}010](0001)$ basal-plane slip system is more active.

Bond-length relaxations were also studied for materials strained from elasticity to structural instability. The relatively weak Ti–Al bonds are demonstrated to accommodate strain dominantly when the materials reach the limit of structural stability. In contrast, strong covalent Ti–C bonds are rigid and insensitive to the applied shear strain. Furthermore, the differences in ideal shear strengths are interpreted from the stability of weak Ti–Al bonds under the two slip systems that were studied.

A polymorphic phase transformation is predicted along the $[1\bar{2}10](0001)$ shear path for Ti_2AlC. In contrast, no polymorphic phase transformation is observed for the $[\bar{1}010](0001)$ shear mode, because the Ti_2C slabs do not hold the original NaCl-type structure and, in addition, Al layers change from hexagonal to cubic stacking in the shear deformed lattice.

Acknowledgments

This work was supported by the National Outstanding Young Scientist Foundation for Y C Zhou under Grant No. 59925208, and the Natural Sciences Foundation of China under Grant Nos 50232040, 90403027 and 50302011.

References

[1] Barsoum M W 2000 *Prog. Solid State Chem.* **28** 201
[2] Pietzka M A and Schuster J C 1994 *J. Phase Equilib.* **15** 392
[3] Wang X H and Zhou Y C 2003 *Oxidation Met.* **59** 303
[4] Wang J Y and Zhou Y C 2004 *Phys. Rev.* B **69** 214111
[5] Salama I, El-Raghy T and Barsoum M W 2002 *J. Alloys Compounds* **347** 271
[6] Farber L, Barsoum M W, Zavaliangos A and El-Raghy T 1998 *J. Am. Ceram. Soc.* **8** 1677
[7] Barsoum M W, Farber L and El-Raghy T 1999 *Metall. Mater. Trans.* A **30** 1727
[8] Jhi S H, Ihm J, Louie S G and Cohen M L 1999 *Nature* **399** 132
[9] Clatterbuck D M, Chrzan D C and Morris J W Jr 2003 *Acta Mater.* **51** 2271
[10] Roundy D, Krenn C R, Cohen M L and Morris J W Jr 1999 *Phys. Rev. Lett.* **82** 2713
[11] Ogata S, Hirosaki N, Kocer C and Shibutani Y 2003 *J. Mater. Res.* **18** 1168
[12] Van V K J, Li J, Zhu T, Yip S and Suresh S 2003 *Phys. Rev.* B **67** 104105
[13] Segall M D, Lindan P L D, Probert M J, Pickard C J, Hasnip P J, Clark S J and Payne M C 2002 *J. Phys.: Condens. Matter* **14** 2717
[14] Vanderbilt D 1990 *Phys. Rev.* B **41** 7892
[15] Perdew J P, Cherary J A, Vosko S H, Jackson K A, Pederson M R, Singh D J and Fiolhais C 1992 *Phys. Rev.* B **46** 6671
[16] Monkhorst H J and Pack J D 1977 *Phys. Rev.* B **16** 1748
[17] Wang J Y and Zhou Y C 2004 *Phys. Rev.* B **69** 144108
[18] Wang J Y, Zhou Y C, Lin Z J, Meng F L and Li F 2005 *Appl. Phys. Lett.* **86** 101902
[19] Sun Z M, Music D, Ahuja R and Schneider J M 2005 *J. Phys.: Condens. Matter* **17** 7169
[20] Hug G and Fries E 2002 *Phys. Rev.* B **65** 113104
[21] Tatsumi K, Tanaka I, Tanaka K, Inui H, Yamaguchi M, Adachi H and Mizuno M 2003 *J. Phys.: Condens. Matter* **15** 6549
[22] Wang Z W, Zha C S and Barsoum M W 2004 *Appl. Phys. Lett.* **85** 3453
[23] Omloo W P F A M and Jellinek F 1970 *J. Alloys Compounds* **20** 121
[24] Bem D S, Lampe-Onerud C M, Olsen H P and zur Loye H C 1996 *Inorg. Chem.* **35** 581